

Supplementary Information

ICT based water-soluble fluorescent probe for discriminating mono and dicarbonyl species and food analysis

Anal Jana, Mousumi Baruah[#], Subrata Munan[#] and Animesh Samanta^{*}

Molecular Sensors and Therapeutics Research Laboratory, Department of Chemistry, School of Natural Sciences, Shiv Nadar University, NH-91, Tehsil Dadri, Gautam Buddha Nagar, UP, India 201314.

[#] Equal contribution

^{*} Corresponding author: animesh.samanta@snu.edu.in

Table of Contents

Sr. No.	Description	Pg. No.
1	General information about the materials used	3
2	General instrumentations	3
3	Synthesis of DANS	3
4	Synthesis of DASH	4
5	Synthesis of DAS	4
6	Proposed mechanism of the formation of DASH	5
7	DEPT ¹³ C NMR spectra of DANS and DASH and comparative ¹ H NMR of DAN, DANS, DASH, DAS	5
8	Photophysical studies	6
8.1	Spectroscopic studies	6
8.2	Relative quantum yield measurements	7
9	Comparative emission spectra of DAN and DAS	7
10	The Solvent-dependent photophysical property of DAS	8
11	Steady-state absorbance and emission spectra of DAS and time-dependent absorbance spectra of DAS in presence of various RCSs	8
12	Time-dependent emission spectra of DAS in presence of FA	9
13	Time dependent emission spectra of DAS in presence of MGO	9
14	Time dependent emission spectra of DAS in presence of GO	10
15	Secondary plot of time-dependent emission spectra of DAS	10
16	Proposed schematic representation of sensing mechanism	11
17	FT-IR spectroscopy of DAS in the presence of RCSs	11
18	NMR based titration of DAS in the presence of FA	11
19	Efficiency of DAS towards RCSs	12
20	Quantum chemical studies	12
21	Determination of the Limit of Detections (LOD)	14
22	pH Dependency of DAS towards detection of RCSs	15
23	Selectivity of DAS towards other reactive analytes	16
24	HepG2 Cell Culture Experiments for cytotoxicity and Bio-Imaging applications	17
24.1	Bio-compatibility of DAS towards HepG2 cell line	17
24.2	Bio-imaging application of DAS	18
25	Application of DAS towards the analysis of food samples and paper-based analysis	20
26	Mass-spectrometric study	21
27	Nuclear Magnetic Resonance (NMR) spectroscopy	22
28	Comparative analysis of previous work and this work	25
29	References	27

1. General information about the materials used

1,8-diamino naphthalene (**DAN**) was obtained from Sigma Aldrich (MO, USA). Concentrated Sulfuric acid and sodium hydroxide pellets were purchased from Fisher Scientific, Mumbai, India. Phosphate buffer saline (PBS) tablets and glyoxal (GO) 40% solution were procured from Loba Chemicals, Mumbai, India. Formaldehyde (FA) solution 37% stabilized by methanol was obtained from Merck KGaA, Darmstadt, Germany. Methylglyoxal (MGO) 30.4% solution was bought from Alfa Aesar (Thermo Fisher (Kan-del) GmbH), Kandel Germany. Dimethyl sulphoxide (DMSO) and other HPLC grade solvents were obtained from Chemlabs, Mumbai, India. DMSO-*d*₆ and D₂O were procured from Eurisotop, France. Dulbecco's modified Eagle's medium (DMEM), 10% fetal bovine serum (FBS) and 100 U penicillin /0.1 mg/ml streptomycin antibiotics were also procured from HiMedia Laboratories, Mumbai and Gibco, Thermo Fisher, UK respectively. Unless otherwise mentioned all the chemicals and the solvents were used as obtained without further purifications.

2. General Instrumentations

The NMR spectra of the synthesized molecules were studied in the Bruker Avance 400 NMR spectrometer, Germany, after diluting in deuterated solvents. The mass spectrometric analysis was studied in Agilent 6540, Q-TOF LC/MS system (Agilent Technologies, Santa Clara, CA, USA) connected with Agilent 1290 UPLC. DI water and acetonitrile along with 0.1% TFA were used as mobile phase with gradient solvent system. The absorption spectra were measured in an Agilent Cary 8454 UV-Vis diode array spectrophotometer. The photoluminescence spectra were measured in Edinburgh FS5 spectrofluorometer (Edinburgh Instruments, Livingstone, United Kingdom; 150 W CW ozone free xenon arc lamp with fully automated filter wheels in the excitation and emission monochromators). The scan slits for excitation and emission were adjusted to 1.2 nm. For biological experiments, cells were incubated in a Thermo Fisher CO₂ incubator and the images were captured in a NIKON Ti-U inverted fluorescence microscope.

3. Synthesis of DANS

In an oven-dried round-bottomed flask, 1 g of 1,8 diamino naphthalene was stirred at 90 °C in 10 ml concentrated Sulfuric acid for overnight. Then the brown mixture was very cautiously added dropwise to the ice-cold water after completion of the reaction. Brownish white precipitation was filtered and washed with ice-cold water until the washing solvents (filtrates) were neutralized that was confirmed with pH paper. The brownish solid was dried in a vacuum

oven overnight and characterized through NMR and HRMS. ^1H NMR (400 MHz, DMSO) δ 7.65 (d, $J = 7.5$ Hz, 1H), 7.42 (t, $J = 7.8$ Hz, 1H), 7.26 – 7.20 (m, 1H). ^{13}C NMR (100 MHz, DMSO) δ 136.02, 135.85, 126.30, 124.60, 120.15, 118.87. HRMS (ESI-QTOF) (M+H)⁺ obtained 239.0489, Calcd. 239.0485.

4. Synthesis of DASH

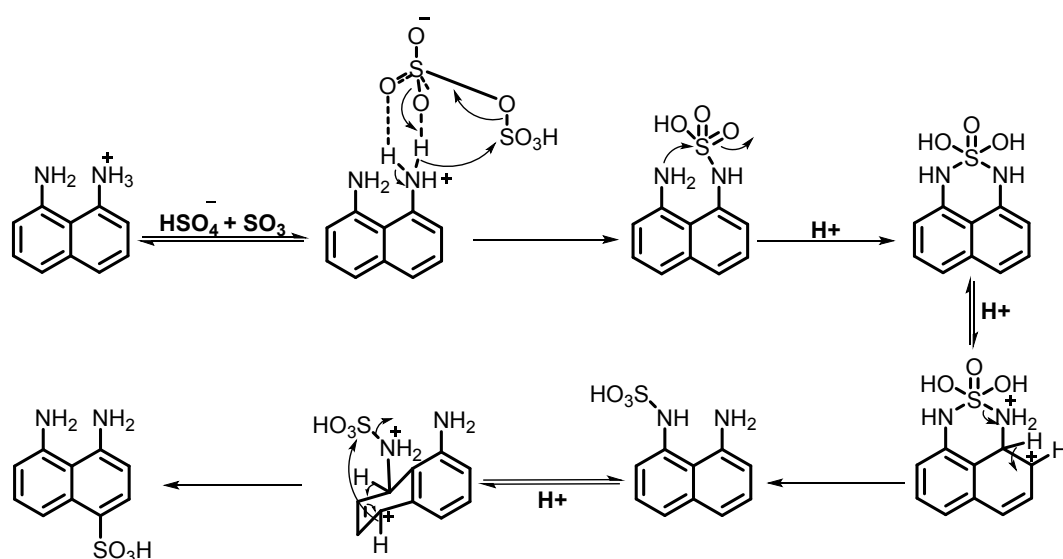
In an oven-dried round-bottomed flask, 1 g of 1,8 diamino naphthalene was stirred at 120 °C in 10 ml concentrated Sulfuric acid overnight. Then the brown mixture was cautiously added dropwise to the ice-cold water after completion of the reaction. Brownish white precipitation was filtered and washed with ice-cold water until the filtrate was neutralized. The brownish solid obtained was dried in a vacuum oven overnight and characterized through NMR and HRMS. ^1H NMR (400 MHz, DMSO) δ 8.69 (d, $J = 8.7$ Hz, 1H), 7.83 (d, $J = 7.8$ Hz, 1H), 7.40 (dd, $J = 8.6, 7.4$ Hz, 1H), 7.25 – 7.21 (m, 1H), 7.00 (d, $J = 7.8$ Hz, 1H). ^{13}C NMR (100 MHz, DMSO) δ 140.17, 138.44, 133.17, 131.95, 125.75, 125.61, 125.29, 120.04, 119.23, 115.44. HRMS (ESI-QTOF) (M+H)⁺ obtained 239.0486, Calcd. 239.0485.

5. Synthesis of DAS

In an oven-dried round-bottomed flask 500 mg **DASH** was stirred with 10 ml of H₂O and after five minutes of stirring few drops of 10% NaOH solution was added dropwise until a clear solution appeared. The reaction mixture was stirred for another 10 minutes and dried in a lyophilizer to get **DAS** with a quantitative yield. ^1H NMR (400 MHz, DMSO) δ 8.06 (d, $J = 8.4$ Hz, 1H), 7.57 (d, $J = 7.9$ Hz, 1H), 7.20 – 6.93 (m, 1H), 6.60 (d, $J = 7.2$ Hz, 1H), 6.40 (d, $J = 7.9$ Hz, 1H), 5.75 (s, 1H), 5.26 (s, 1H). ^{13}C NMR (100 MHz, DMSO) δ 148.03, 146.04, 133.36, 133.13, 126.36, 125.82, 118.46, 115.06, 111.21, 107.23. HRMS (ESI-QTOF) (M+H)⁺ obtained 239.0305, Calcd. 239.0304. (N.B.: The mass spectrometric analysis showed exactly equal mass value as **DASH**, because of using 0.1% formic acid solution as mobile phase.)

Caution: Concentrated H₂SO₄ is a strong inorganic acid and capable of burn the skin and can cause permanent blindness if come in direct contact of eyes. Utmost care should be taken during usage of this strong acid.

6. Proposed mechanism of the formation of DASH



Scheme S1. Plausible mechanism of the formation of **DASH** from **DAN** in presence of concentrated H_2SO_4 . This proposed mechanism is based on the reported p-sulfonation of aniline upon heating H_2SO_4 ¹.

7. DEPT ^{13}C NMR spectra of **DANS** and **DASH** and Comparative ^1H NMR of **DAN**, **DANS**, **DASH**, **DAS** and

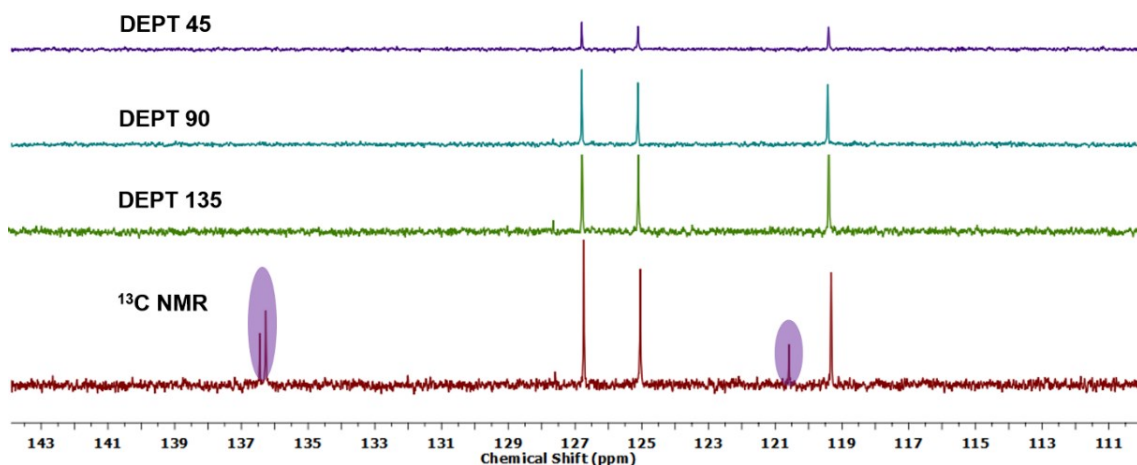


Fig. S1: DEPT NMR spectra of **DANS**. The presence of four quaternary aromatic carbon confirms that there is no sulfonation occurs at the aromatic ring.

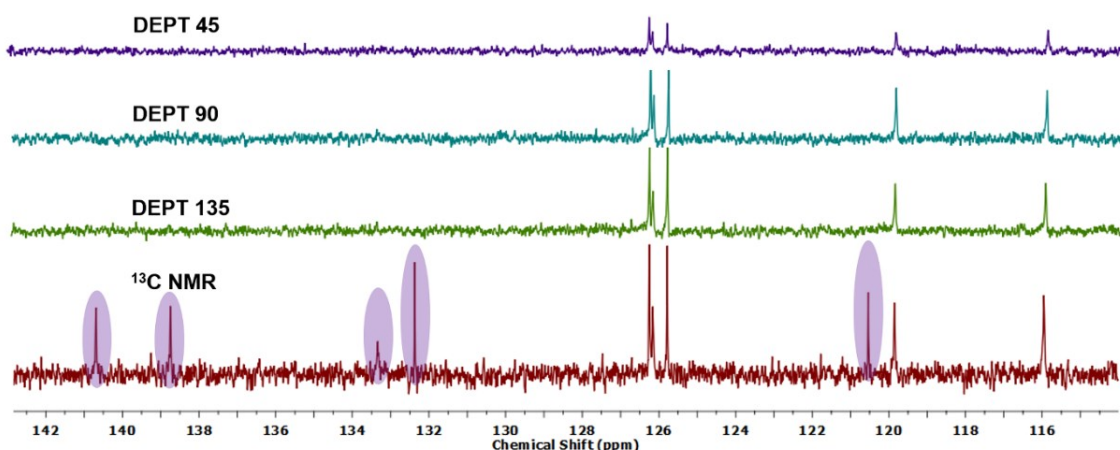


Fig. S2: DEPT NMR spectra of **DASH**. The unsymmetrical nature of carbon NMR along with five quaternary carbon further confirms the presence of a C-Sulphonated molecule.

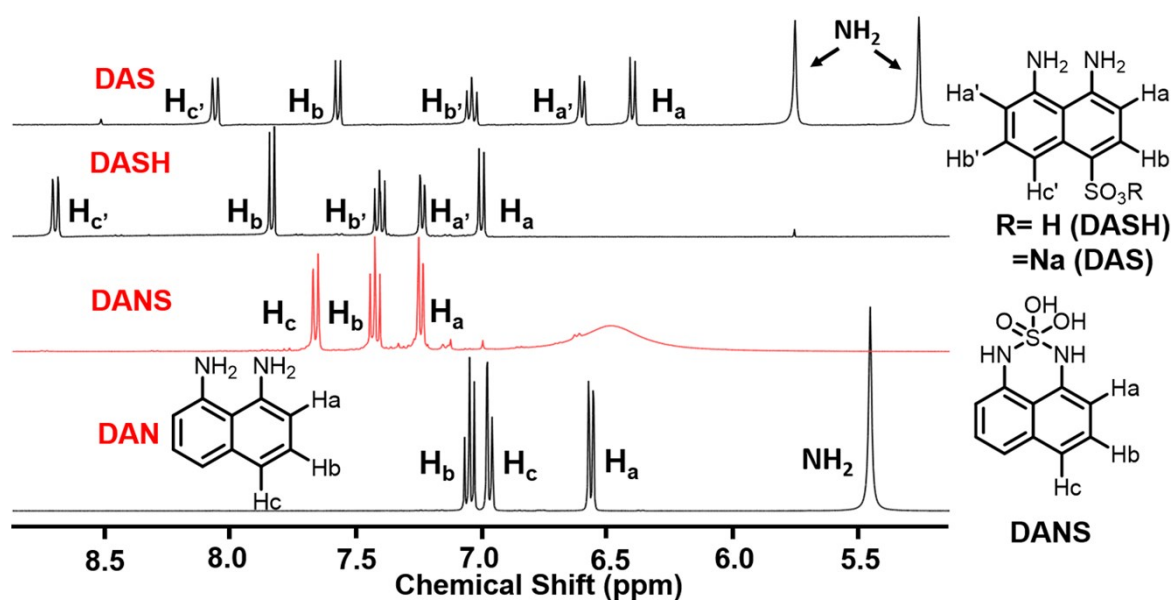


Fig. S3: Comparative NMR spectra of **DAN**, **DANS**, **DASH** and **DAS** in the $\text{DMSO-}d_6$ solvent. Symmetrical nature of the spectra is changed upon the formation of **DASH** which further shifted in the up-field region upon the formation of **DAS**.

8. Photophysical studies

8.1 Spectroscopic studies

The steady-state photophysical properties of **DAS** were studied by UV-Vis and photoluminescence spectrophotometry. Firstly, a 5 mM stock solution of **DAS** was prepared in PBS (10 mM, pH 7.4). Further, the stock solution was diluted to the final experimental concentration in PBS buffer (10 mM, pH 7.4). All the spectroscopic studies such as absorption,

solvent-dependent studies in HPLC grade solvents. A 5 mM stock solution in DMSO was prepared for the solvent dependent experiments and used in such a way so that the final DMSO concentration remains not more than 0.1% in respective solvents. 10 mM PBS buffer solution of pH 7.4 was measured as a blank solution before steady-state and the time-dependent UV-Vis kinetics studies. The time-dependent absorption study was conducted in the kinetics mode of the instrument and recorded the absorption wavelength in each 30 seconds interval. Steady-state time-dependent emission spectra were evaluated at 345 nm excitation wavelength at 5 min time interval. Concentration dependents experiments were performed similarly at different incubation times, with similar parameters.

8.2 Relative quantum yield measurements

Relative fluorescence quantum yields of **DAS** alone and **DAS** along with the RCSs were measured by taking **DAN** as a reference (6.01%)². Quantum yields were calculated by using the following formula:

$$\Phi_X = \Phi_{ST} \left(\frac{Grad_X}{Grad_{ST}} \right) \left(\frac{\eta^2_X}{\eta^2_{ST}} \right) \quad (\text{Eq. 1})$$

Where Φ_X is the quantum yield of the sample, Φ_{ST} is the quantum yield of the standard. $Grad_X$ and $Grad_{ST}$ is the gradient of the plot of the area under the curve of the emission spectra of samples and standards respectively and η represents the refractive index of respective solutions. The calculated relative quantum yield for **DAS** is found to be 5.2%.

9. Comparative emission spectra of DAN and DAS

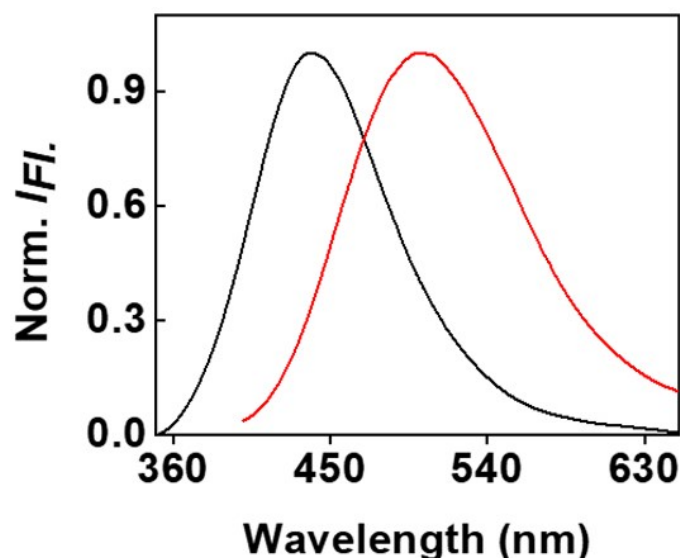


Fig. S4: Comparative emission spectra of **DAN** (black) and **DAS** (red) in PBS (10 mM, pH 7.4) shows a shift in λ_{max} from 440 nm to 507 nm with 67 nm increased Stokes's shift. This large bathochromic shift is due to the strong ICT from donor (amines) to acceptor (Sulfonate) groups.

10. The Solvent-dependent photophysical property of DAS

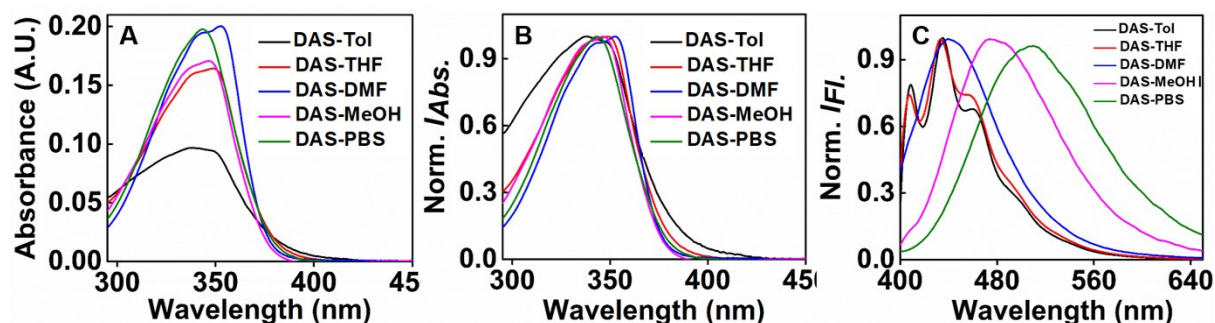


Fig. S5: Solvent dependent UV-Vis spectroscopy of **DAS** (20 μM) and Normalized emission spectra of **DAS** (5 μM) in different solvents. Clear redshifted emission spectra in the polar solvent further confirmed the enhanced charge transfer nature of the molecule.

11. Steady-state absorbance and emission spectra of DAS and time-dependent absorbance spectra of DAS in presence of various RCSs

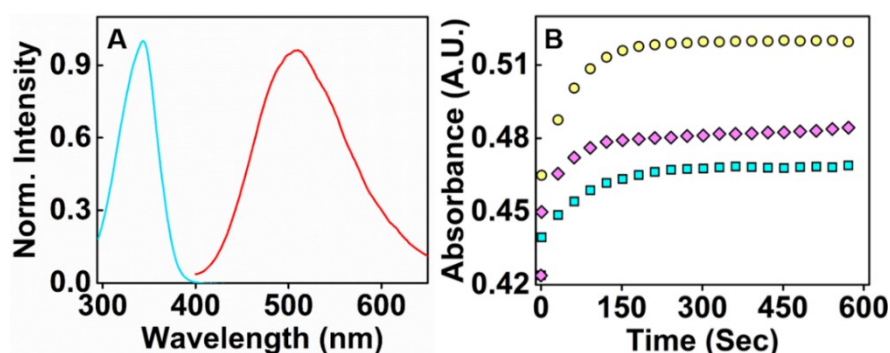


Fig. S6: A) Steady-state normalized absorbance and emission spectra of **DAS** in PBS (10 mM, pH 7.4) buffer showing an improved Stoke's shift of 157 nm. B) Time-dependent change of absorbance intensity of **DAS** (50 μM) at wavelength 345 nm in the presence of 300 μM of FA (cyan), MGO (yellow) and GO (pink) showing a gradual increase of absorbance intensity at 345 nm.

12. Time-dependent emission spectra of DAS in presence of FA

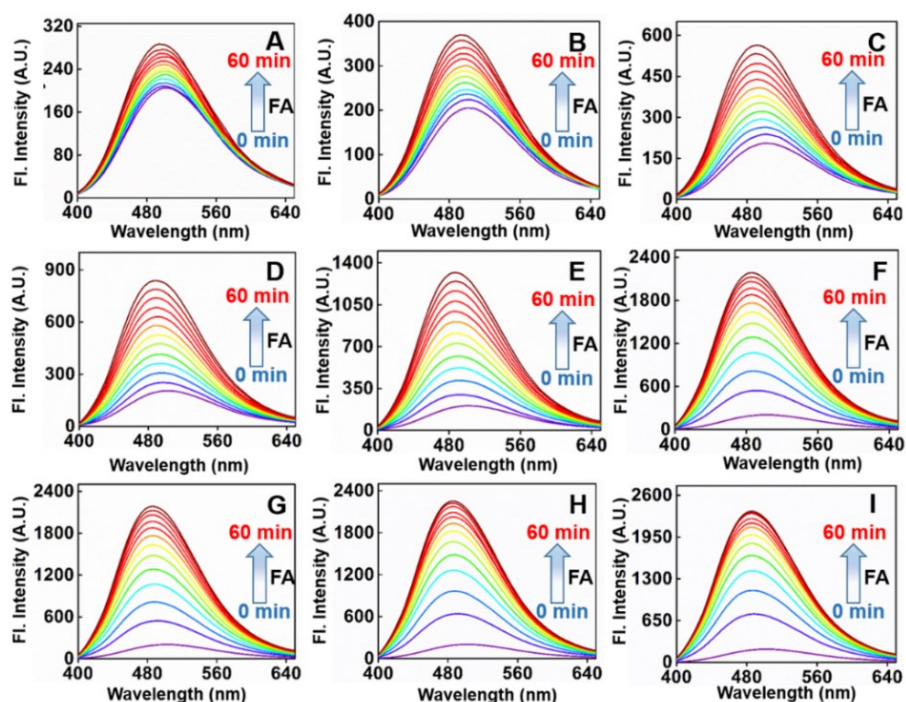


Fig. S7: Time dependent emission spectra of **DAS** (5 μM) in PBS (10 mM, pH 7.4) in presence of various concentration of FA (A) 10 μM , (B) 20 μM , (C) 50 μM , (D) 100 μM , (E) 200 μM , (F) 400 μM , (G) 600 μM , (H) 800 μM , (I) 1000 μM .

13. Time dependent emission spectra of DAS in presence of MGO

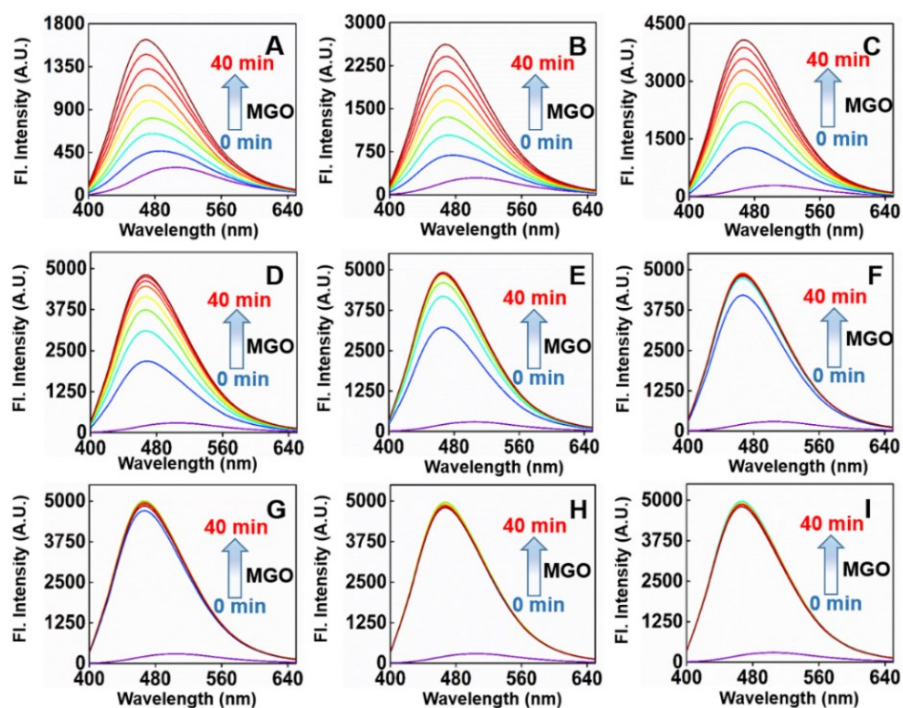


Fig. S8: Time dependent emission spectra of DAS ($5 \mu\text{M}$) in PBS (10 mM , pH 7.4) in presence of various concentration of MGO (A) $10 \mu\text{M}$, (B) $20 \mu\text{M}$, (C) $50 \mu\text{M}$, (D) $100 \mu\text{M}$, (E) $200 \mu\text{M}$, (F) $400 \mu\text{M}$, (G) $600 \mu\text{M}$, (H) $800 \mu\text{M}$, (I) $1000 \mu\text{M}$.

14. Time dependent emission spectra of DAS in presence of GO

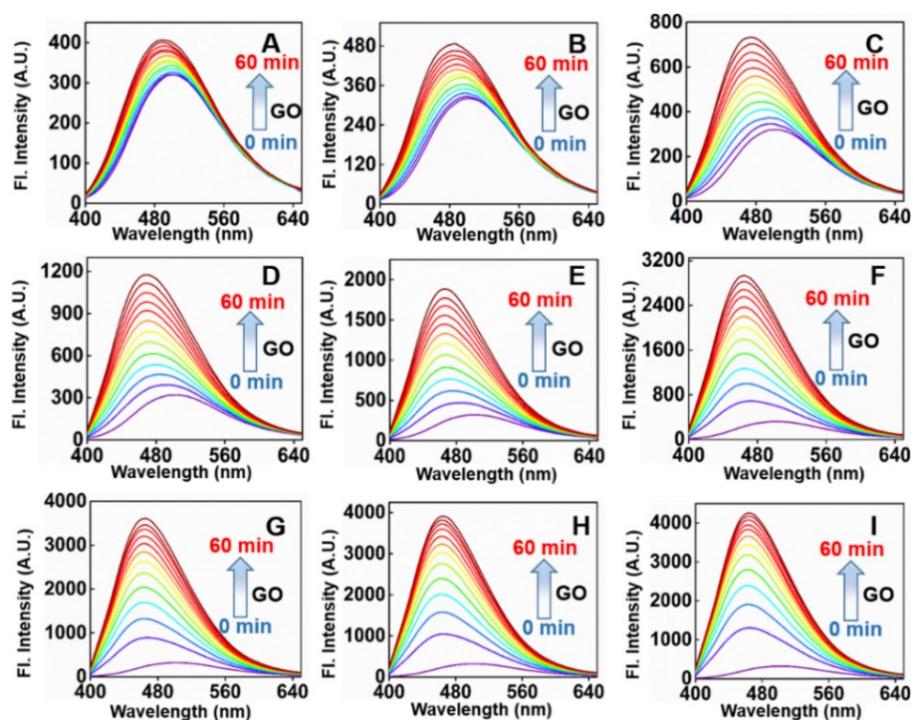


Fig. S9: Time dependent emission spectra of **DAS** (5 μM) in PBS (10 mM, pH 7.4) in presence of various concentration of GO (A) 10 μM , (B) 20 μM , (C) 50 μM , (D) 100 μM , (E) 200 μM , (F) 400 μM , (G) 600 μM , (H) 800 μM , (I) 1000 μM .

15. Secondary plot of time-dependent emission spectra of DAS

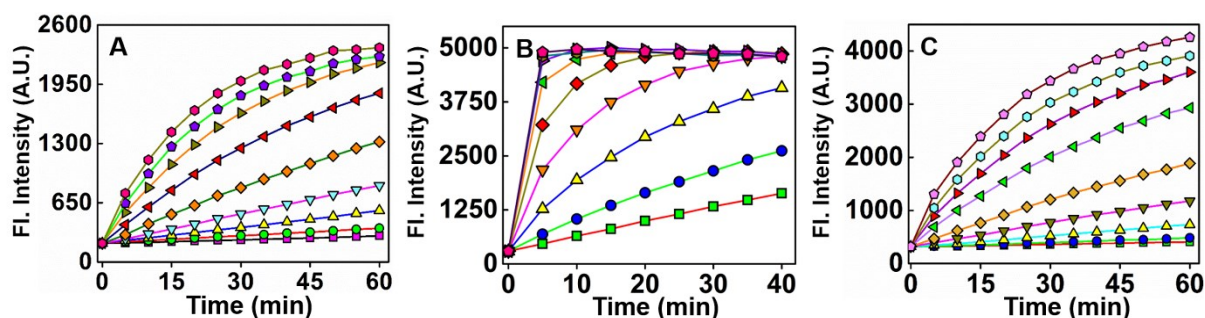
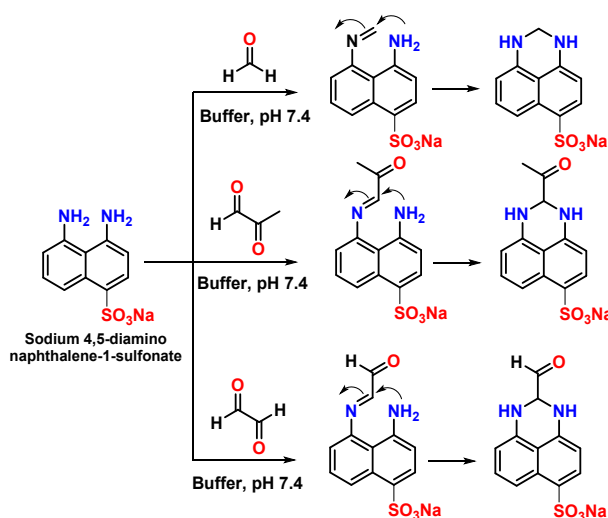


Fig. S10: Secondary plot of time-dependent emission spectra of **DAS** in the presence of A) FA B) MGO and C) GO at various concentrations.

16. Proposed schematic representation of sensing mechanism



Scheme S2: The proposed schematic representation of the sensing mechanism of **DAS** in presence of FA, MGO and GO.

17. FT-IR spectroscopy of DAS in the presence of RCSs

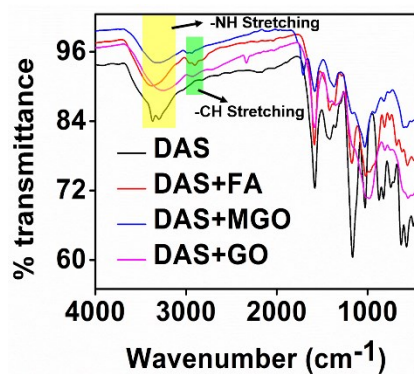


Fig. S11: FTIR spectroscopy of **DAS** and **DAS** in the presence of RCSs (FA, MGO and GO).

18. NMR based titration of DAS in the presence of FA

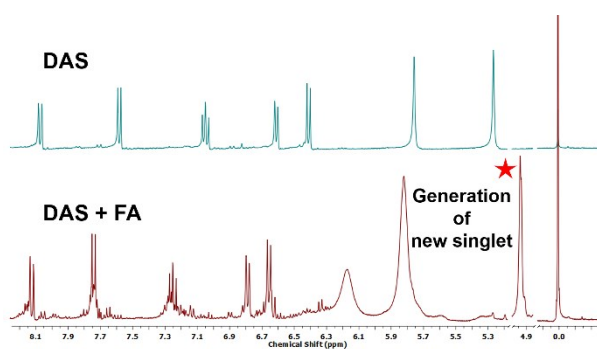


Fig. S12: ^1H NMR titration experiment of **DAS** with FA was found to a new singlet peak at 4.93 ppm which was assigned as the methylene peak in pyrimidine structure. However, we have tried the similar experiments with MGO and GO also but due to the presence of several interfering peaks at similar position we are unable to detect any new peak. The experiment was done by addition of FA in a solution of DAS in $\text{DMSO-}d_6$ and measuring the NMR spectrum after 2 hr of incubation.

19. Efficiency of DAS towards RCSs

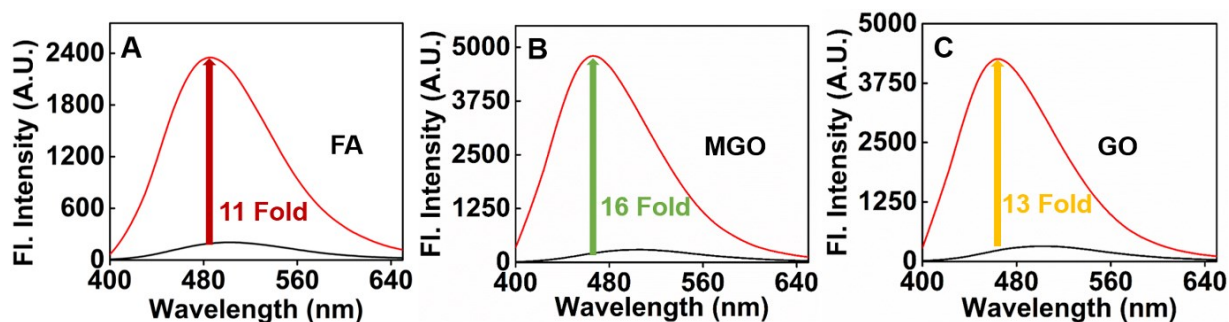


Fig. S13: Fold of enhancement of emission intensity of **DAS** (5 μM) in presence of 1mM FA, MGO and GO upon incubation of 60 min in case of FA and GO and 40 min in case of MGO.

20. Quantum chemical studies

Computational calculations of the probe and the possible products were done in a Gaussian 09, Revision of D.01 software package installed at Magus High-Performance Cluster (HPC) computing facility in SNU.¹² The ground state structures were optimized at B3LYP³ level of theory using 6-31+G (d, p)⁴ basis set taking water as the solvent through the polarizable continuum model (PCM)⁵ to mimic the aqueous environment.

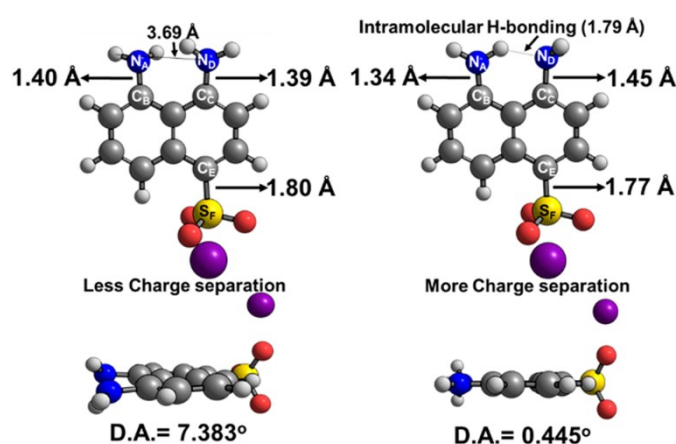


Fig. S14: Increased charge separation along with excited state H-bonding interaction in **DAS** facilitates the ICT process with increased planarity in the excited state.

The excited-state properties of the systems were calculated using time-dependent density functional theory (TD-DFT)^{6,7} from the coordinates of the ground state optimized structures using B3LYP³ as the level of theory with 6-31+G (d, p) basis sets in PCM model taking water as the solvent. The excitation energy of the systems was calculated in a non-equilibrium solvation model whereas the excited state energy levels were calculated considering the equilibrium solvation model with corrected linear response (cLR) methodology⁸. The bond orders in the ground state, as well as the excited states, were calculated with natural bond orbital (NBO) calculation version 3.1 installed in the Gaussian software package using B3LYP level of theory with 6-311++G(d, p) basis set⁹.

The optimized ground state geometry of **DAS** showed a dihedral angle of 7.383° along the $\text{N}_\text{A}\text{C}_\text{B}\text{C}_\text{C}\text{N}_\text{D}$ plane which upon excitation showed an improved planarity with a reduction of the dihedral angle to 0.445° that further facilitate the transfer of charge inside the molecule.

Further the TD-DFT calculations showed that a lower HOMO-LUMO band gap of 3.30 eV in the case of **DAS** with an oscillator strength of 0.01660. However, upon reaction with FA the HOMO-LUMO energy gap was further increased to 3.61 eV with an increased oscillator strength. It was observed that the gap was somewhat decreased in the case of dicarbonyl species which should actually red-shift the emission spectra. However, a close insight showed the oscillator strength for the HOMO-LUMO transition in the case of MGO and GO was only 0.0080 and 0.0013 respectively. In the case of dicarbonyl species actually HOMO-LUMO+1 transition was occurring along with a higher oscillator strength of 0.3439 and 0.3522 for the case of MGO and GO respectively. The energy differences of these orbitals were further increased compared to **DAS** and **DAS-FA** and showed a blue shift in the emission spectrum.

The efficient charge transfer mechanism was also supported by the excited state bond order calculation using NBO 3.1 software package installed in Gaussian 09.¹³ From the Table S1 it can be well understood that N_C-N_D bond order was somewhat higher in the ground state, indicating a transfer of charge from N_C to the acceptor sulfonate group. However, in the excited state the reverse trend was observed, i.e., increased N_A-C_B bond order was observed. This further indicate a higher separation of charge leading to an efficient intra molecular charge transfer in the system. Further it was also observed that the extent of charge transfer was somewhat lower indicated by relatively smaller N_A-C_B bond order increment in the case of **DAS-RCS** molecules compare to **DAS** which pointed towards the blue shift of the emission spectra in terms of lowered ICT process.

	$N_A C_B C_C N_D$		N_A-C_B		N_D-C_C	
	Dihedral Angle		Bond Order		Bond Order	
	G.S	E.S	G.S	E.S	G.S	E.S
DAS	7.383	0.445	0.9453	1.0360	0.9648	0.8722

DAS-FA	0.823	9.399	0.9516	0.9944	0.9659	0.9457
DAS-MGO	0.434	2.291	0.9378	1.0109	0.9343	0.9857
DAS-GO	0.319	0.460	0.9275	1.0013	0.9438	0.989

Table S1. Ground state (G.S) and excited state (E.S) dihedral angle and bond order parameters of **DAS** and in presence of FA, MGO and GO.

21. Determination of the Limit of Detections (LOD)

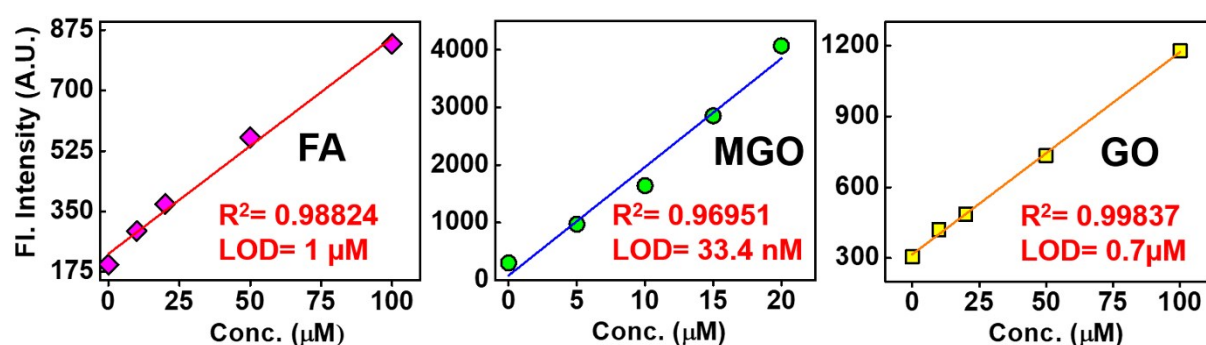


Fig. S15: Determination of Limit of Detection (LOD) of **DAS** in presence of RCSs. Calculated LOD for FA is $1 \mu\text{M}$, for MGO was 33.4 nM and for GO was $0.7 \mu\text{M}$.

The limit of detection (LOD) for **DAS** towards FA, MGO, and GO (RCSs) were calculated using Eq. 2:

$$\text{Limit of Detection (LOD)} = 3\sigma/\text{slope} \text{ (Eq. 2)}$$

where σ standard deviation of 10 blank measurements and slope obtained from the graph of fluorescence intensity vs concentration of RCSs at lower concentrations.

22. pH Dependency of DAS towards detection of RCSs

The emission spectra of **DAS** were measured in presence different RCSs in different time of incubation, i.e., 15 minutes and 45 minutes in PBS buffer (10 mM, pH 7.4). pH dependent emission was found to be remaining silent in biological pH window (pH 4-9) made the probe effective for bio-imaging throughout the entire biological pH window. However, the “turn on” response towards RCSs was much prominent in the acidic region (pH \sim 4) compared to basic (pH 9). As **DAS** does not respond to acidic pH but showed better response towards RCSs in

the acidic region indicating the formation of Schiff base followed by cyclization. At pH ~4, the aminium ion in **DAS** participated in neighboring proton transfer (NPT) to activate RCSs resulting in faster Schiff base formation followed by cyclization to enhance the fluorescence intensity.

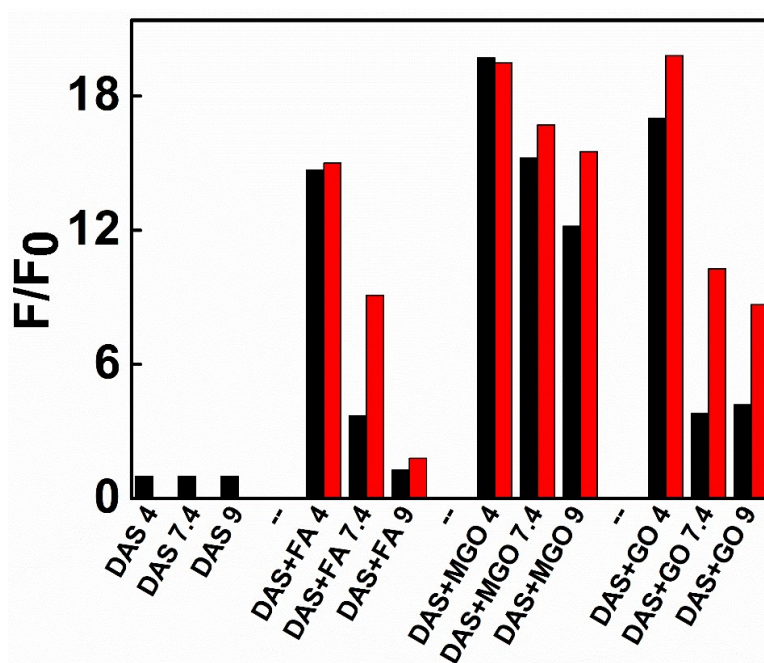


Fig. S16: Dependency of **DAS** on pH towards detection of RCSs at different time of incubation. (15 minutes, black), 45 minutes, red).

23. Selectivity of DAS towards other reactive analytes

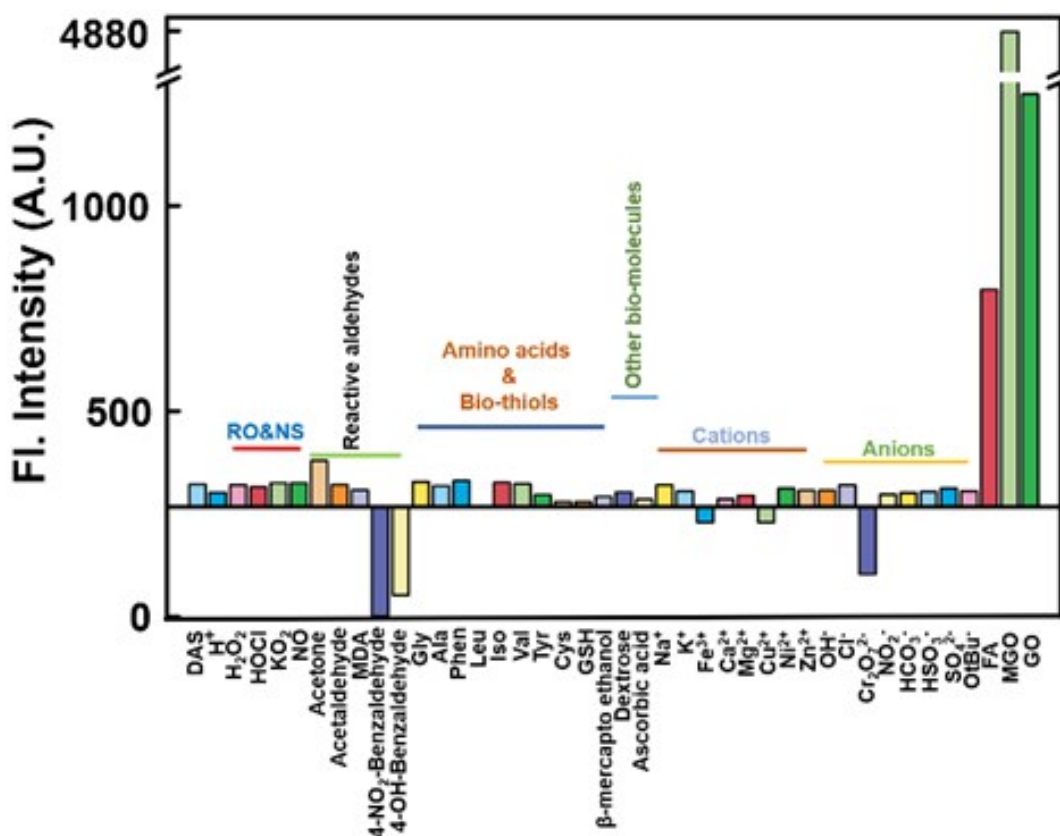


Fig. S17: The selectivity study of DAS towards other probable interfering analytes.

The selectivity of DAS towards other interfering analytes was monitored in terms of emission spectra. The selectivity of the probe was ensured towards other relevant reactive carbonyls such as acetaldehyde, benzaldehyde, 4-hydroxy benzaldehyde and 4-nitro benzaldehyde along with FA, MGO and GO. In addition, various reactive oxygen and nitrogen species (H₂O₂, HOCl, KO₂ and NO); relevant amino acids (Gly, Ala, Phe, Leu, Iso, Val) and relevant bio thiols (Cys, GSH, β-Mercaptoethanol) and other bio molecules such as dextrose, ascorbic acid etc. were also verified. The probe was also subjected to treat with various relevant cations (Na⁺, K⁺, Fe³⁺, Ca²⁺, Mg²⁺, Cu²⁺, Ni²⁺ and Zn²⁺) and anions (OH⁻, Cl⁻, Cr₂O₇²⁻, NO₃⁻, HCO₃⁻, HSO₃⁻, SO₄²⁻ and O^tBu⁻). In this experiment the probe was incubated with the relevant analyte of a concentration of 300 μM and the emission intensity was measured by exciting at 345 nm. It was found the probe is very much selective towards these RCSs (FA, MGO and GO) and for the other analytes it remains either silent, minimal change or showed a quenching property. A slight increase in the emission intensity was observed in the case of acetone, however owing to the stronger +I effect the reaction is much slower in comparison to the FA, MGO and GO. Thus, DAS is selected as a promising “turn on” fluorescent probes for monitoring exogenous RCSs (FA, GO

and MGO) in cellular conditions and preserved food analysis by determining FA and the quantification of antimicrobial MGO in Manuka honey.

24. HepG2 Cell Culture experiments for cytotoxicity and Bio-Imaging applications

Human hepatocellular carcinoma cell line HepG2 was a generous gift from Dr. Deepak Sehgal's lab of Dept. of Life Sciences, Shiv Nadar University. Cells were maintained in DMEM with 10% FBS and 1% Pen-Strep under an atmosphere of 5% CO₂ at 37 °C. The biocompatibility of the probe was determined in terms of standard MTT [(3-(4,5-Dimethylthiazol-2-yl)-2-5- Diphenyl tetrazolium Bromide)] assay before subjecting the DAS for the imaging experiments. The procedures for cellular experiments are described in the supporting materials.

24.1. Bio-compatibility of DAS towards HepG2 cell line

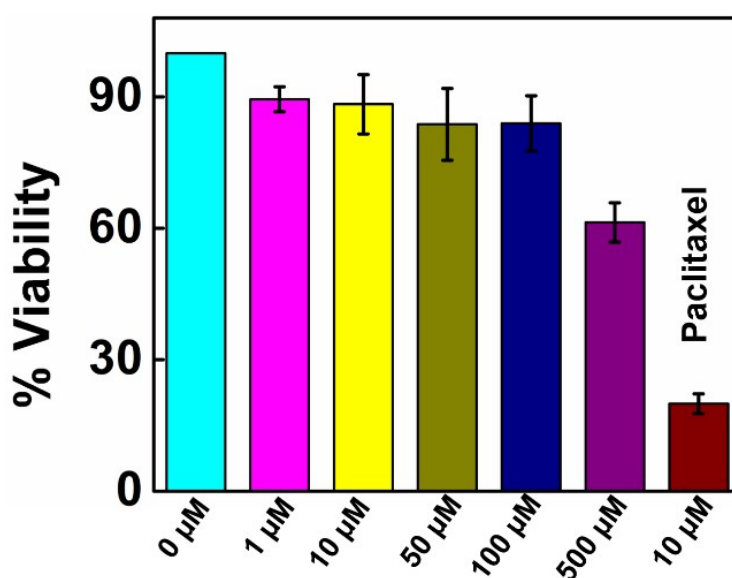


Fig. S18: Biocompatibility study of DAS in terms of standard MTT assays taking Paclitaxel as a positive control.

Cellular compatibility of the probe initially was measured in terms of MTT, [(3-(4,5-Dimethylthiazol-2-yl)-2-5- Diphenyl tetrazolium Bromide)] assay as described previously. Briefly in a 96 well plates 5000 cells were incubated for 24 hrs followed by treatment of the adhered cells with the required concentrations of DAS and 10 μM of Paclitaxel was taken as a positive control and incubated under similar environment for another 24 hrs. After incubation 10% final concentration of MTT solutions (As delivered and instructed by Hi-Media

Laboratory, Mumbai, India) and incubated for 4 hrs with constant monitoring of the needle shaped crystal appearance with a Leica microscope. After incubation media were removed carefully and 100 μ l of solubilisation buffer was added and further incubated for 30 minutes until complete dissolution of the crystals. After that absorbance were measure at 595 nm and the % of cell viability was calculated using the formula:

$$\text{Viability (\%)} = \text{Abs. sample/Abs. control} \times 100$$

24.2 Bio-imaging applications of DAS

Before each imaging experiment cells were treated with required concentration of RCSs and incubated for 60 minutes. After incubation cells were washed with PBS buffer for two times and treated with 100 μ M of **DAS** and incubated for another 60 minutes. After incubation the plates were washed three times with PBS buffer to remove any extra probes followed by images were taken in a NIKON Ti-U inverted fluorescence microscope with 40X magnification. The image background was further removed using ROI background removal method of ImageJ software and then quantified.

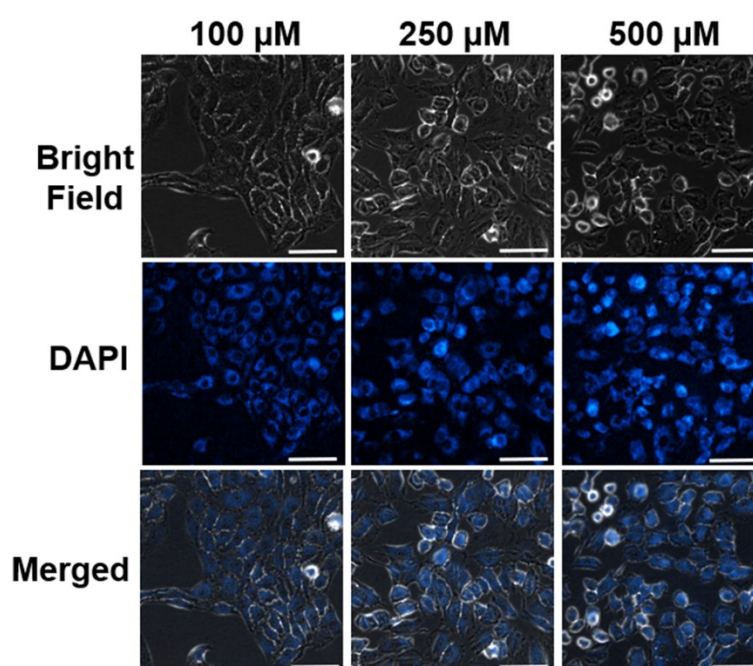


Fig. S19: Concentration dependent bioimaging of exogenous FA by **DAS**.

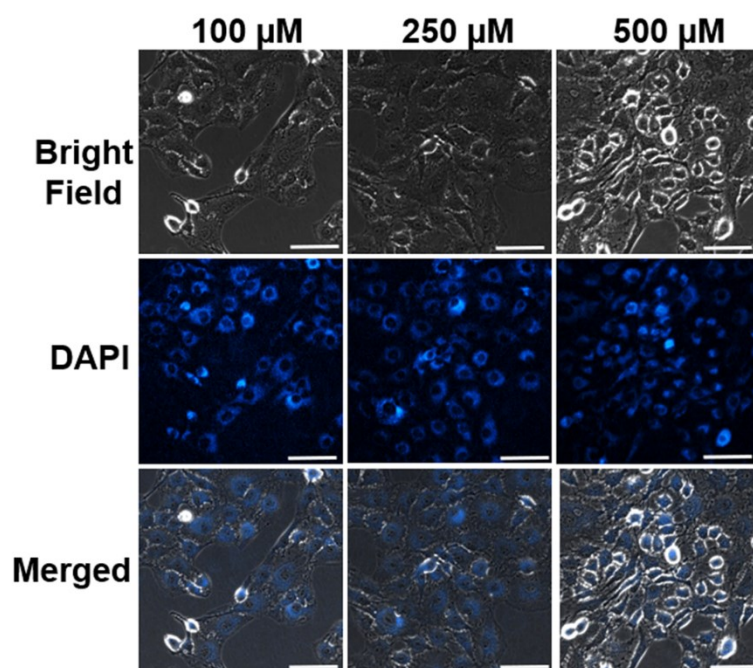


Fig. S20: Concentration dependent bioimaging of exogenous MGO by DAS.

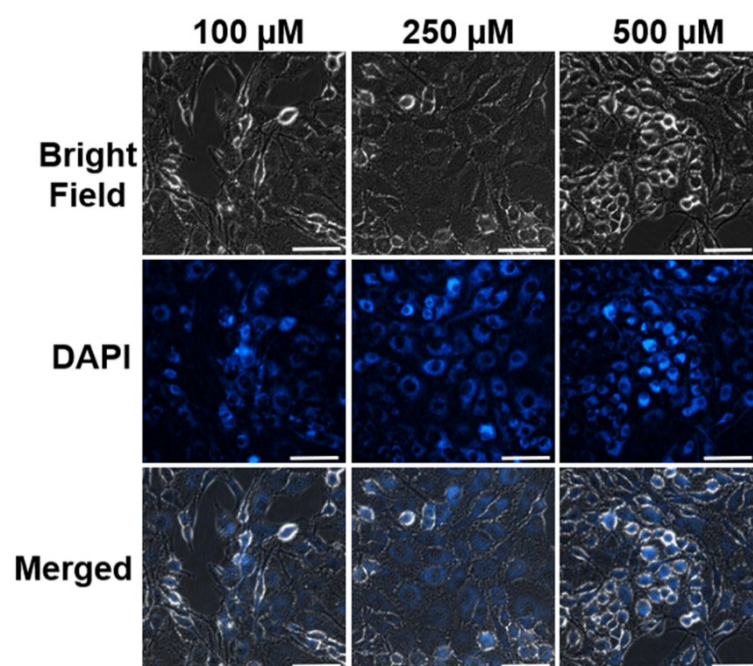


Fig. S21: Concentration dependent bioimaging of exogenous GO by DAS.

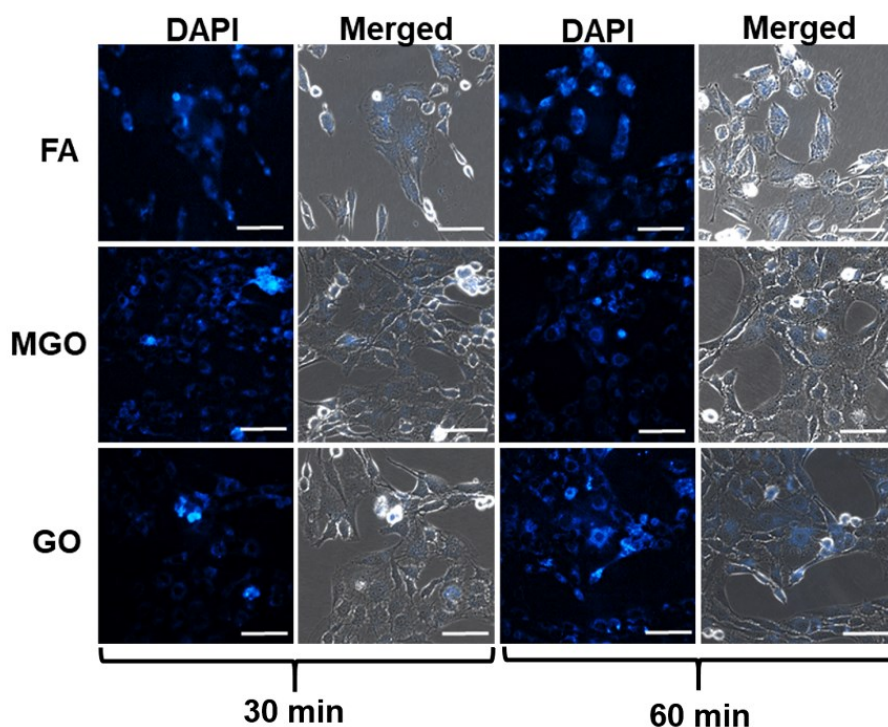


Fig. S22: Time dependent cellular images of **DAS** in upon addition of 500 μM of RCSs.

25. Application of **DAS** towards the analysis of food samples and paper-based analysis

It is well known that the FA is regularly used in the preservation of raw fish and chicken. For FA detection in fish and chicken samples, we have bought raw fish and chicken from the local market and 2 g of each sample were prepared by slightly modifying the protocol as described by Ding et. al.¹⁰ After extraction in PBS buffer (10 mM, pH 7.4) 20 μL of the extracted solution was mixed with 5 μM **DAS** and incubated for 10 minutes and the emission intensity was measured to detect the emission enhancement. Control samples were also studied without adulterated them with FA.

After getting confirmed about the ability of **DAS** for the detection of FA from the preserved food sample, we checked its ability to quantify the amount of the preservative used. For this we prepared a standard calibration curve in terms of fold of enhancement and the concentration of the FA and studied one unknown sample (previously intoxicated with $\sim 5\%$ FA solution) and correlated its fold of enhancement with the concentration of FA used. We found that the concentration is exactly matched with the theoretical value and from this experiment we can confirm that **DAS** can be used for quantify the unknown FA concentration in the real food samples.

To further evaluate the ability of **DAS** towards the detection of MGO in honey samples we have diluted the honey with hot water in a ratio of 3:7 (Honey: Water) and 200 μL of this solution was incubated for 30 minutes with 5 μM of **DAS** and quantified with the developed standard calibration curve at similar incubation time¹¹.

We have also investigated the ability of **DAS** towards detection and discrimination among the reactive mono and dicarbonyls on test strips in liquid phase. A distinguishable emission color change of the paper strips in presence of monocarbonyl, FA and dicarbonyl MGO was observed under 365 nm UV exposure. However, in the vapor phase only in presence of FA a distinguishable color change was observed but almost no change of color in case of MGO or GO due to their high boiling points.

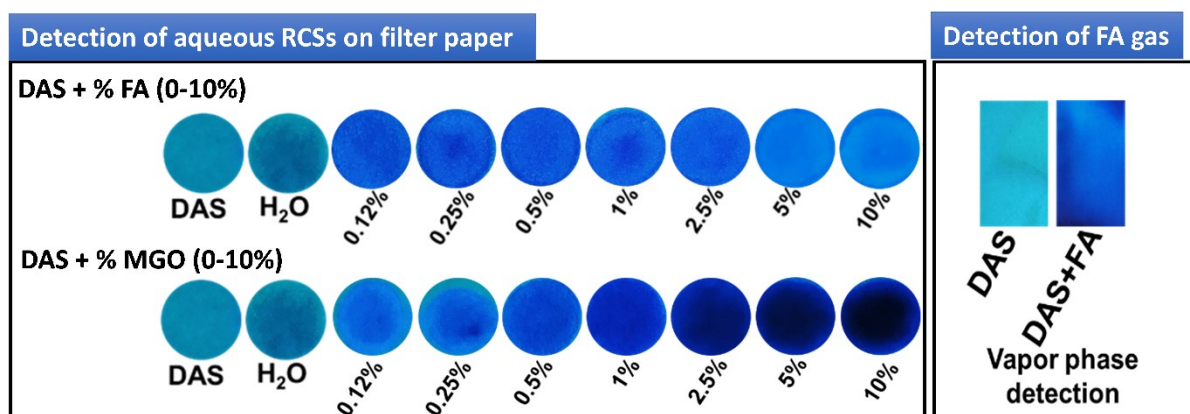


Fig S23: Detection of monocarbonyl and the dicarbonyl species in the aqueous and vapor phase by DAS loaded paper strips under the exposure of 365 nm UV light.

26. Mass-spectrometric study

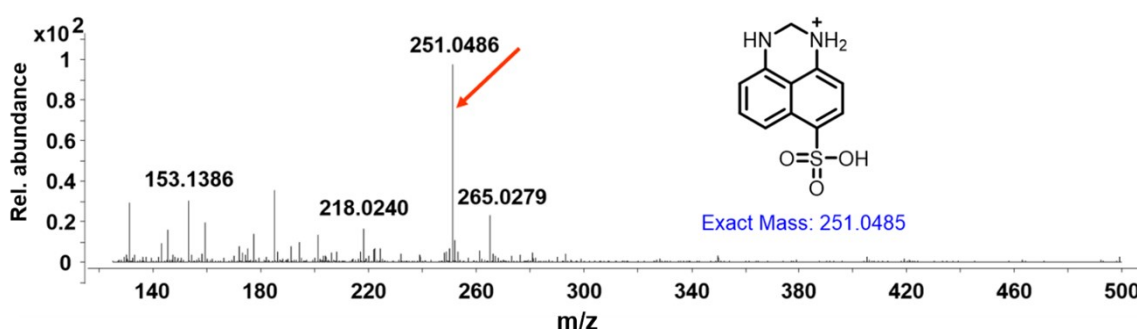


Fig. S24: ESI-HRMS study of **DAS** in presence of FA.

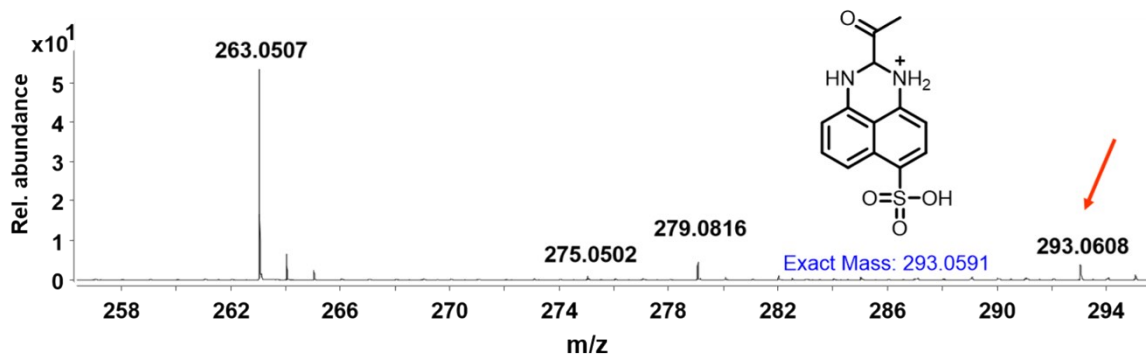


Fig. S25: ESI-HRMS study of DAS in presence of MGO.

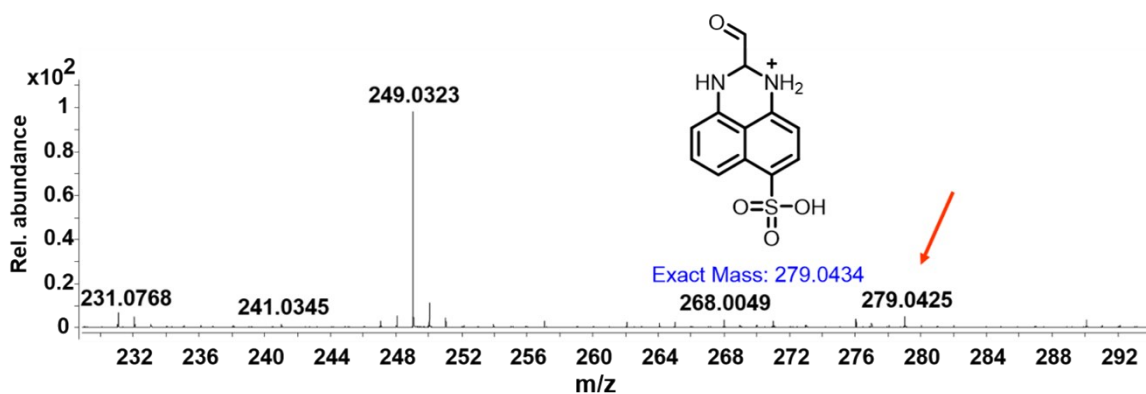


Fig. S26: ESI-HRMS study of DAS in presence of GO.

27. Nuclear Magnetic Resonance (NMR) spectroscopy

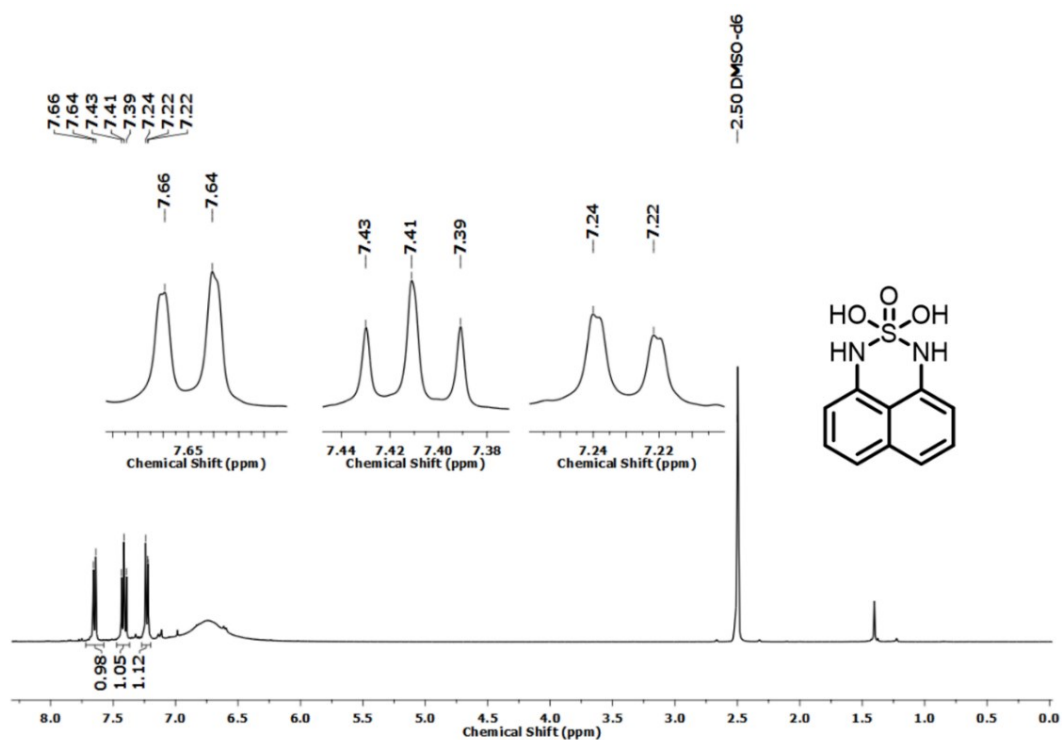


Fig. S27: ^1H NMR of DANS.

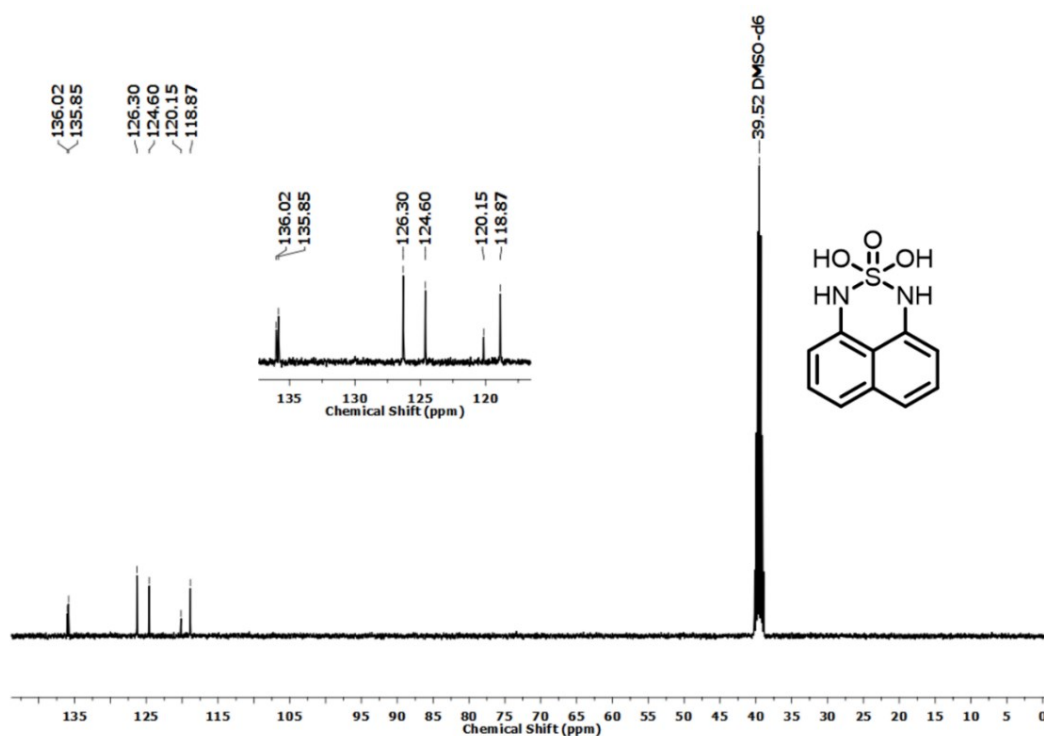


Fig. S28: ^{13}C NMR of DASH.

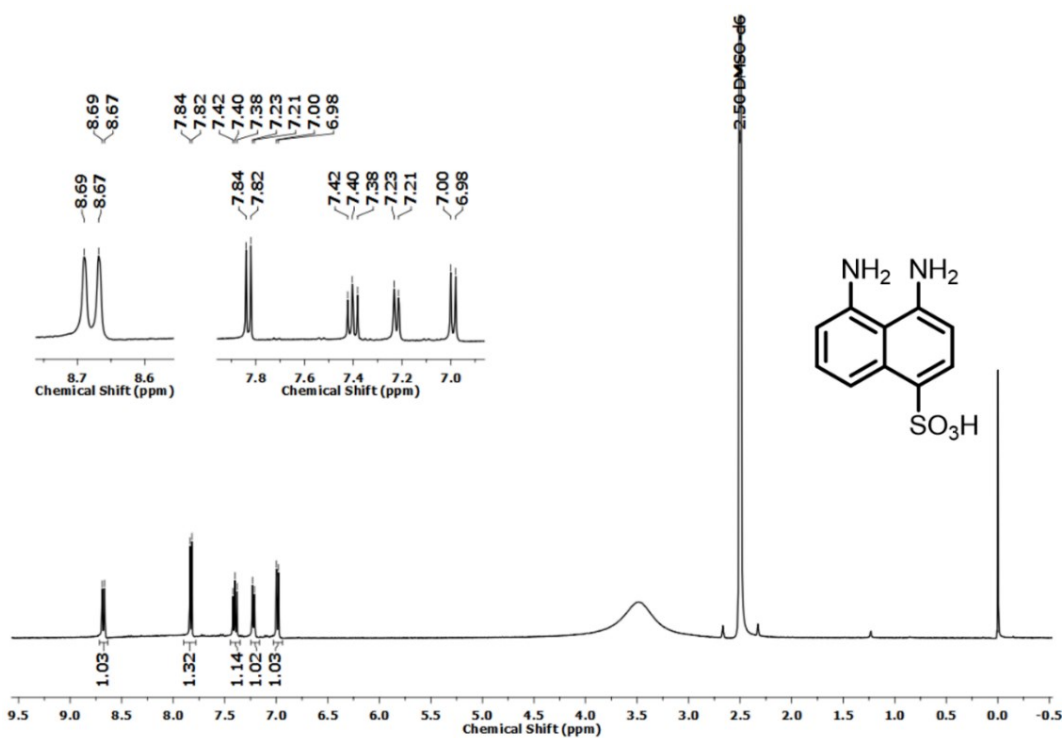


Fig. S29: ^1H NMR of DASH.

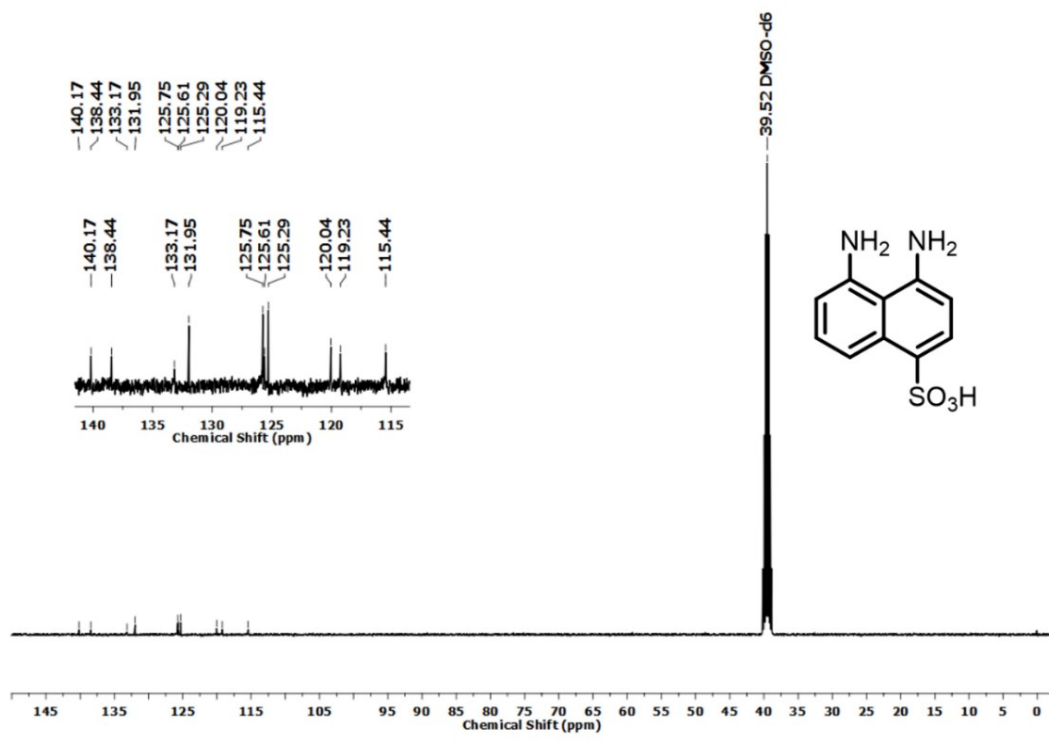


Fig. S30: ¹³C NMR of DASH.

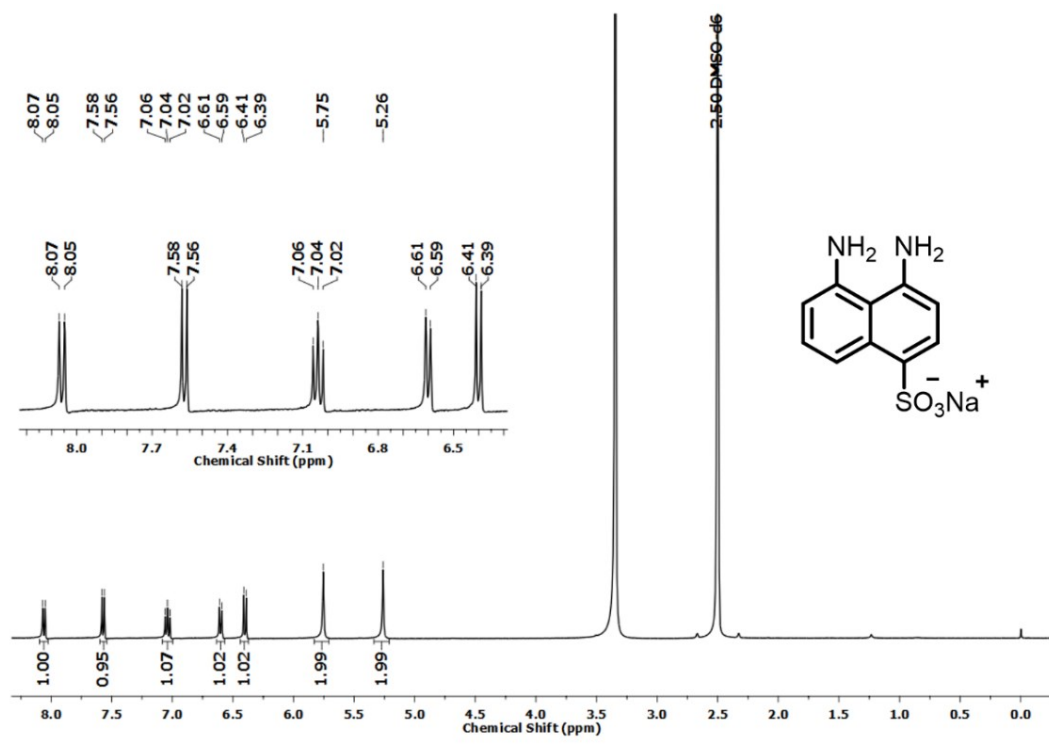


Fig. S31: ¹H NMR of DAS.

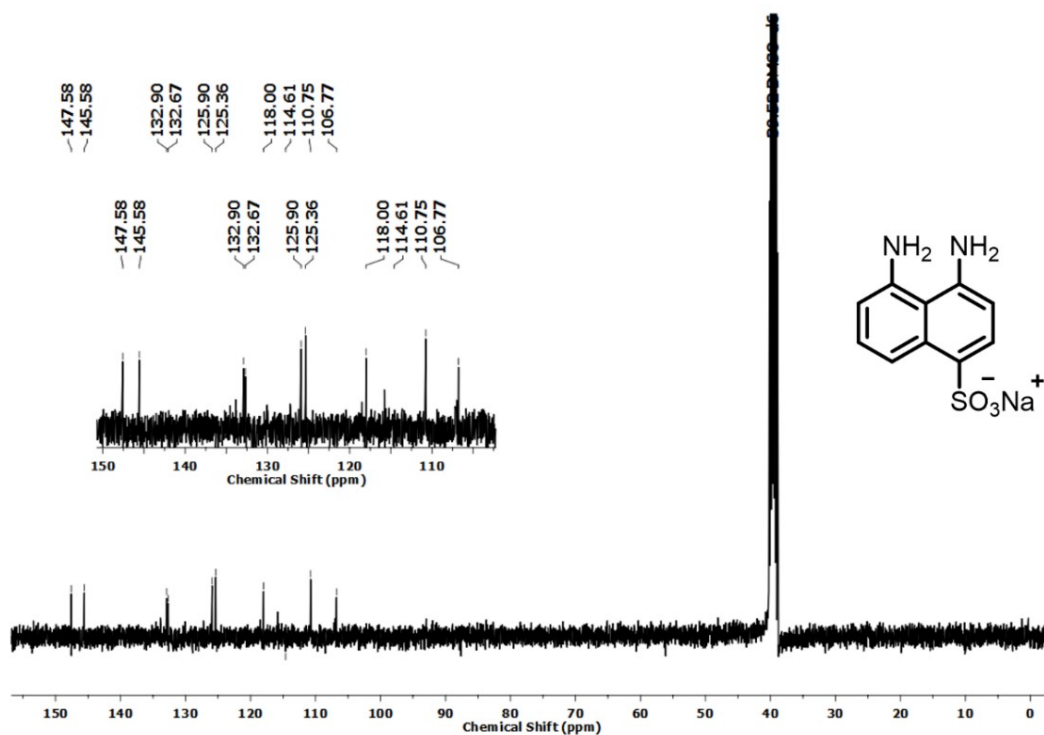
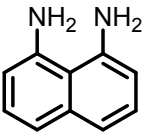
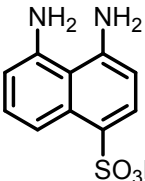


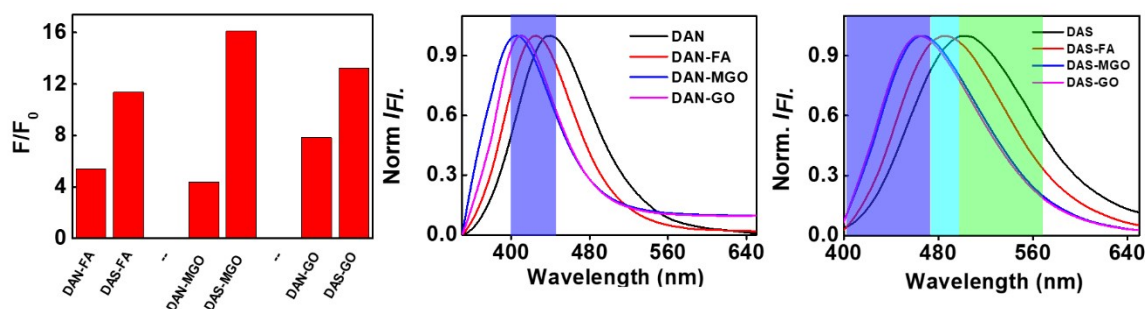
Fig. S32: ^{13}C NMR of DAS.

28. Comparative analysis of previous work and this work

Table S2:

Our previous work:		This work:	
 <p>DAN</p>	Solvent: PBS/0.1% DMSO LOD for FA: 0.95 μM LOD for MGO: 1.31 μM LOD for GO: 3.97 μM	 <p>DAS</p>	Solvent: Water or Buffer LOD for FA: 1 μM LOD for MGO: 33.4 nM LOD for GO: 0.7 μM

Comparison in term of Fold of enhancement and spectral shift:

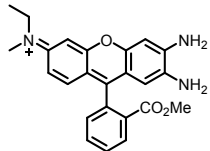
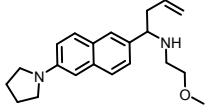
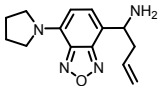


	λ_{Em} Wavelength (nm)	λ_{Em} in presence of FA (nm)	λ_{Em} in presence of MGO (nm)	λ_{Em} in presence of GO (nm)
DAN	441	424 (16)	404 (37)	411 (30)
DAS	507	490 (17)	465 (42)	465 (42)

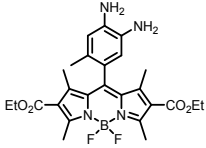
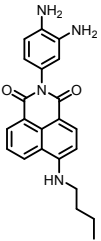
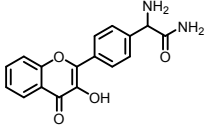
Table S3:

Selective fluorescence probe for FA

Structure	Solvent	Response time	LOD	Appl.	Ref
	PBS	3 Hr	0.01 mM	HEK293T N and NS1	J. Am. Chem. Soc. 2015, 137, 10890–10893
	PBS, 1% DMSO	Within 10 min	7.1×10^{-7} M	HeLA/ Liver	Angew. Chem. Int. Ed. 2016, 55, 3356–3359
	Aq. Buffer.	10 second	7.7×10^{-7} M	HeLA	Chem. Commun., 2016, 52, 9582

	Tris-HCl, 30% EtOH	30 min	8.3 μM	L929	Dyes and Pigments 138 (2017) 23-29
	PBS buffer	n/a	10 μM	Cells and tissues	Anal. Chem. 2017, 89, 3724–3731
	PBS, 20% ACN	150 min	4.35 $\times 10^{-8}$ & 4.97 $\times 10^{-8}$ M	HeLa	New J. Chem., 2018, 42, 12361-12364

Selective Fluorescence probe for methylglyoxal

Structure	Solvent	Response time	LOD	Applications	Ref
	PBS	60 min	50- 100 nM	HeLa	J. Am. Chem. Soc. 2013, 135, 12429–12433
	PBS/ DMSO	-	1.47 μM	HeLa	J. Fluoresc., 2018, 29, 155– 163
	PBS/ 10 % DMSO	90 min	0.24- 0.5 μM	HeLa/Blood	Anal. Chem. 2019, 91, 5646–5653

29. References:

- 1 Z. Vrba and Z. J. Allan, *Tetrahedron Lett.*, 1968, **9**, 4507–4510.
- 2 A. R. Al-Betar, A. El-Rayyes and U. K. A. Klein, *J. Fluoresc.*, 2005, **15**, 689–696.

- 3 L. S. Kassel, *J. Chem. Phys.*, 1936, **4**, 276–282.
- 4 J. E. Del Bene, W. B. Person and K. Szczepaniak, *J. Phys. Chem.*, 1995, **99**, 10705–10707.
- 5 B. Mennucci, J. Tomasi, R. Cammi, J. R. Cheeseman, M. J. Frisch, F. J. Devlin, S. Gabriel and P. J. Stephens, *J. Phys. Chem. A*, 2002, **106**, 6102–6113.
- 6 C. Adamo and D. Jacquemin, *Chem. Soc. Rev.*, 2013, **42**, 845–856.
- 7 A. D. Laurent, C. Adamo and D. Jacquemin, *Phys. Chem. Chem. Phys.*, 2014, **16**, 14334–14356.
- 8 M. Caricato, B. Mennucci, J. Tomasi, F. Ingrosso, R. Cammi, S. Corni and G. Scalmani, *J. Chem. Phys.*, 2006, **124**, 124520.
- 9 I. Alkorta, I. Rozas and J. Elguero, *Struct. Chem.*, 1998, **9**, 243–247.
- 10 H. Ding, G. Yuan, L. Peng, L. Zhou and Q. Lin, *J. Agric. Food Chem.*, 2020, **68**, 3670–3677.
- 11 J. M. Alvarez-Suarez, M. Gasparrini, T. Y. Forbes-Hernández, L. Mazzoni and F. Giampieri, *Foods (Basel, Switzerland)*, 2014, **3**, 420–432.
- 12 Gaussian 09, Revision D.01, M. J. Frisch, G. W. Trucks, H. B. Schlegel, G. E. Scuseria, M. A. Robb, J. R. Cheeseman, G. Scalmani, V. Barone, B. Mennucci, G. A. Petersson, H. Nakatsuji, M. Caricato, X. Li, H. P. Hratchian, A. F. Izmaylov, J. Bloino, G. Zheng, J. L. Sonnenberg, M. Hada, M. Ehara, K. Toyota, R. Fukuda, J. Hasegawa, M. Ishida, T. Nakajima, Y. Honda, O. Kitao, H. Nakai, T. Vreven, J. A. Montgomery, Jr., J. E. Peralta, F. Ogliaro, M. Bearpark, J. J. Heyd, E. Brothers, K. N. Kudin, V. N. Staroverov, T. Keith, R. Kobayashi, J. Normand, K. Raghavachari, A. Rendell, J. C. Burant, S. S. Iyengar, J. Tomasi, M. Cossi, N. Rega, J. M. Millam, M. Klene, J. E. Knox, J. B. Cross, V. Bakken, C. Adamo, J. Jaramillo, R. Gomperts, R. E. Stratmann, O. Yazyev, A. J. Austin, R. Cammi, C. Pomelli, J. W. Ochterski, R. L. Martin, K. Morokuma, V. G. Zakrzewski, G. A. Voth, P. Salvador, J. J. Dannenberg, S. Dapprich, A. D. Daniels, O. Farkas, J. B. Foresman, J. V. Ortiz, J. Cioslowski, and D. J. Fox, Gaussian, Inc., Wallingford CT, 2013.

13 NBO Version 3.1, E. D. Glendening, A. E. Reed, J. E. Carpenter, and F. Weinhold.